International Journal of Automation and Computing 11(4), August 2014, 441-448
DOI: 10.1007/s11633-014-0811-8

Compressive Sensing Inverse Synthetic Aperture Radar Imaging Based on Gini Index Regularization

Can Feng[1, 2] Liang Xiao[1] Zhi-Hui Wei[1]

[1]School of Computer Science and Engineering, Nanjing University of Science & Technology, Nanjing 210094, China
[2]North Information Control Group Co., Ltd., Nanjing 211153, China

Abstract: In compressive sensing (CS) based inverse synthetic aperture radar (ISAR) imaging approaches, the quality of final image significantly depends on the number of measurements and the noise level. In this paper, we propose an improved version of CS-based method for inverse synthetic aperture radar (ISAR) imaging. Different from the traditional l_1 norm based CS ISAR imaging method, our method explores the use of Gini index to measure the sparsity of ISAR images to improve the imaging quality. Instead of simultaneous perturbation stochastic approximation (SPSA), we use weighted l_1 norm as the surrogate functional and successfully develop an iteratively re-weighted algorithm to reconstruct ISAR images from compressed echo samples. Experimental results show that our approach significantly reduces the number of measurements needed for exact reconstruction and effectively suppresses the noise. Both the peak sidelobe ratio (PSLR) and the reconstruction relative error (RE) indicate that the proposed method outperforms the l_1 norm based method.

Keywords: Compressive sensing, inverse synthetic aperture radar (ISAR) imaging, sparsity, Gini index, regularization.

1 Introduction

Inverse synthetic aperture radar (ISAR) has been proven to be a powerful signal processing technique for imaging moving targets in range and cross-range domain under all-weather circumstances[1−3]. ISAR imagery plays an important role in military and civilian applications such as target identification, recognition and classification. In these applications, a critical requirement of the ISAR image is to achieve high resolution in both range and cross-range domains. In conventional ISAR imaging framework, ISAR images are usually obtained using the range-doppler (RD) algorithm which is based on the 2D Fourier transformation[4, 5]. Under this imaging framework, range resolution is proportional to the bandwidth of transmitted signal, and cross-range resolution is dependent on both the coherent processing interval (CPI) as well as the target rotational motion from variation of radar viewing angles[5]. To obtain a considerably high range and cross range resolution targets′ image through RD algorithm, the bandwidth of radar transmitted signal must be sufficiently large and the targets′ observation duration must be long enough.

However, there are several constraints in real ISAR imaging system to acquire a very high range and cross range resolution targets images: 1) Due to system limitations, it is impractical to obtain higher and higher range resolution ISAR images by continually increasing the system bandwidth. 2) Long duration targets observation may be unachievable since targets are usually non-cooperative and maneuvering, and it brings difficulty for the real-time tracker to produce a well-focused image. 3) A large bandwidth and long observation duration produce huge amount of data, and often the data handling is the most crucial matter of radar design.

To overcome those constraints, the recently developed theory of compressive sensing (CS)[6−8] presents a novel way to deal with those problems. CS theory suggests that it is possible to reconstruct a sparse or compressible signal from a small number of compressed measurements with an appropriate nonlinear reconstruction procedure. Unlike Nyquist-Shannon sampling theorem based signal sampling way, CS performs compressed sampling using the sparsity of the signal, which permits signals to be sampled at the sub-Nyquist rate and reconstructed from the limited compressed measurements. In the context of radar signal processing, especially in ISAR signal processing, CS has attracted more and more attentions since one can obtain better performance and easier data acquisition and storage schemes[9−14]. In 2009, Ender[10] presented several generic system architectures of CS based radar and put forth some major open questions related with the application of CS to SAR and ISAR imaging. In [11], a CS-based ISAR imaging algorithm is proposed to estimate locations of scattering centers from very limited measurements. And in [12], the algorithm is improved to overcome strong noise and clutter by combining coherent projectors and weighting with the CS optimization for ISAR image generation. In 2012, Zhao et al.[14] proposed a novel reconstruction model called MCS model deduced from Meridian prior, and with the decrease of the number of pulses and signal-to-noise ratio MCS model exhibits better performance in terms of resolution and amplitude error than that of the Laplace-prior-based CS model.

In most of current literature on CS based ISAR imaging approaches, sparsity of ISAR image is commonly measured by l_1 norm, and ISAR images are reconstructed by solving a l_1 minimization problem. However, in the case of real situation, l_1 norm may not be practical due to following observations. 1) Intuitively, a signal is sparse if its energy

Regular paper
Manuscript received April 12, 2013; revised September 24, 2013
This work was supported by National Natural Science Foundation of China (Nos. 61071146, 61171165 and 61301217), Natural Science Foundation of Jiangsu Province (No. BK2010488) and National Scientific Equipment Developing Project of China (No. 2012YQ050250).

is concentrated in a small number of its coefficients. For instance, we consider the two signals $\boldsymbol{x}_1 = (7, 1, 1, 0)$ and $\boldsymbol{x}_2 = (3, 3, 3, 0)$. Intuitively, the sparsity of $\boldsymbol{x}_1$ should be more than $\boldsymbol{x}_2$, since most of the signal energy in $\boldsymbol{x}_1$ is concentrated in just one element. But in the sense of l_1 norm, the sparsities of $\boldsymbol{x}_1$ and $\boldsymbol{x}_2$ are the same ($\|\boldsymbol{x}_1\|_1 = \|\boldsymbol{x}_2\|_1 = 9$). So, a sparsity measure should depend on the relative distribution of energy among the coefficients. But it should not be calculated solely by the absolute value of each coefficient. 2) A good sparsity measure should be a weighted sum of coefficients of signal representation, based on the importance of a particular coefficient in the overall sparsity. As a consequence, any slight change in the value of a coefficient will affect sparsity only relative to the weight of that coefficient, which is a desirable property. The above two observations raise the question of whether we can improve upon l_1 norm based sparsity measure and l_1 minimization and design a new CS ISAR imaging algorithm to achieve robustness and stability against strong noise.

In this paper, we consider one such alternative. Using the Gini index[15, 16] as a measure of sparsity, we introduce an enhancing sparse recovery model to reconstruct high resolution ISAR image from compressed echo measurements. In contrast to other compressive ISAR related model, this paper, which is an extension of our previous work[17], explores the use of Gini index instead of l_1 nrom to measure the sparsity of ISAR images.

The main contribution of this paper is twofold: 1) By using the Gini index as a measure of sparsity, we propose an enhancing sparse recovery model to construct high resolution ISAR images from compressed echo measurements. 2) An efficient CS imaging algorithm is developed using a novel iteratively reweighed scheme. The results show that our approach significantly reduces the number of measurements needed for exact reconstruction and effectively suppresses the noise, and both the PSLR and RE values indicate that the proposed method outperforms l_1 norm based method.

The rest of paper is organized as follows. In Section 2, we present the ISAR system signal model and review current CS based imaging formation. Section 3 introduces Gini index based ISAR imaging model and algorithm. Experimental results and performance comparison of proposed approach and other current approaches are given in Section 4. Finally, Section 5 concludes the paper.

2 ISAR signal model and imaging via CS

In this section, we present the ISAR system signal model with stepped frequency continuous wave (SFCW) and briefly review the l_1 norm based CS ISAR imaging formation.

2.1 ISAR observation model

We assume that the translational motion has been compensated by conventional methods[18−20] and the transmitted signal of radar system is the stepped frequency continuous wave (SFCW) with m bursts of n pulses. Each frequency component in the burst is $f_i = f_0 + i\triangle f$, $i = 0, 1, 2, \cdots, n-1$, where f_0 is the initial frequency and $\triangle f$ is the frequency step in the burst. The total frequency bandwidth B can be readily calculated as

$$B = f_{n-1} - f_0 + \triangle f = n\triangle f. \tag{1}$$

Let us consider the geometry shown in Fig. 1 where the target is rotating with a rotational velocity of ω. The origin of the geometry is R_0 away from the radar. Assuming that the target is at the far field of the radar, the received signals of the i-th scattering center located at $P(x_i, y_i)$ on the target have the form of[1]

$$E^s(\boldsymbol{f}, \boldsymbol{t}) = \alpha_i \mathrm{e}^{-\mathrm{j}2\pi\left(\frac{2\boldsymbol{f}}{c}\right)R(x_i, y_i, \boldsymbol{t})} + \eta \tag{2}$$

where α_i is the complex magnitude of the i-th scattering center, c is the speed of light, $\boldsymbol{f} = (f_0, f_1, \cdots, f_{N-1})$ is the frequency vector, η is the additional noise, and $R(x_i, y_i, \boldsymbol{t})$ is the instantaneous distance from point scatterer to radar and can be written as

$$R(x_i, y_i, \boldsymbol{t}) = \sqrt{(R_0 + x_i\cos\omega\boldsymbol{t} - y_i\sin\omega\boldsymbol{t})^2 + (x_i\sin\omega\boldsymbol{t} + y_i\cos\omega\boldsymbol{t})^2}. \tag{3}$$

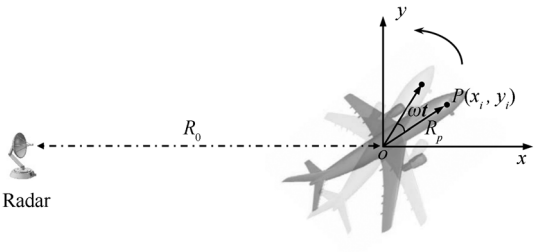

Fig. 1 Geometry for ISAR imaging of a rotating target

Let us assume that the target in Fig. 1 contains p point scatterers located at (x_i, y_i) where i runs from 1 to p. Then, the received signal can be formulated as

$$E^s(\boldsymbol{f}, \boldsymbol{t}) = \sum_{i=1}^{p} \alpha_i \mathrm{e}^{-\mathrm{j}2\pi\left(\frac{2\boldsymbol{f}}{c}\right)R(x_i, y_i, \boldsymbol{t})} + \eta. \tag{4}$$

We should point out that the received echo signal $E^s(\boldsymbol{f}, \boldsymbol{t})$ is complex data, and we assume the noise η is Gaussian distributed complex noise.

Now, we split the imaging scene by N grids denoted by $\{(\tilde{x}_k, \tilde{y}_k)\}_{k=1}^{N}$, and define a dense dictionary as

$$\begin{cases} \boldsymbol{\Psi} = \{\varphi_1, \varphi_2, \cdots, \varphi_N\} \\ \varphi_k(\boldsymbol{f}, \boldsymbol{t}) = \mathrm{e}^{-\mathrm{j}2\pi\left(\frac{2\boldsymbol{f}}{c}\right)R(\tilde{x}_k, \tilde{y}_k, \boldsymbol{t})}, \quad k = 1, 2, \cdots, N. \end{cases} \tag{5}$$

Then the received signal expressed in (4) can be rewritten as

$$E^s(\boldsymbol{f}, \boldsymbol{t}) = \sum_{i=1}^{N} \tilde{\alpha}_i \mathrm{e}^{-\mathrm{j}2\pi\left(\frac{2\boldsymbol{f}}{c}\right)R(\tilde{x}_i, \tilde{y}_i, \boldsymbol{t})} + \eta \tag{6}$$

and it can further be represented as

$$E^s(\boldsymbol{f}, \boldsymbol{t}) = \boldsymbol{\Psi}\boldsymbol{a} + \boldsymbol{\eta} \tag{7}$$

where $\boldsymbol{\Psi} \in \mathbf{C}^{N\times N}$ is a dense dictionary, $\boldsymbol{a} = [\tilde{a}_1, \tilde{a}_2, \cdots, \tilde{a}_N]^{\mathrm{T}}$ is redefined as the vector whose nonzero components correspond to the complex amplitudes of the p strong scatterers.

Inspired by the CS theory, a sensing matrix $\boldsymbol{\Phi} \in \mathbf{C}^{M\times N}$ is applied to decrease the data rate, and we then have the following ISAR signal observation model:

$$E = \boldsymbol{\Phi}\boldsymbol{\Psi}\boldsymbol{a} + \boldsymbol{\eta} \tag{8}$$

where $E \in \mathbf{C}^M$ is the compressed echo measurements.

The ISAR imaging problem is how to reconstruct the reflectivity $\boldsymbol{a}$ from (8). Given E with a low dimension, exact reconstruction of $\boldsymbol{a}$ is challenging as one has fewer equations than unknowns in (8).

2.2 l_1 norm based CS ISAR imaging

Firstly, we give a brief introduction to the concept of compressed sensing. A good overview can be found in [8]. Suppose $\boldsymbol{x} \in \mathbf{C}^N$ is K-sparse in a basis or more generally a dictionary $\boldsymbol{\Psi}$, so that $\boldsymbol{x} = \boldsymbol{\Psi}\boldsymbol{x}_0$, with $\|\boldsymbol{x}_0\|_0 = K \ll N$, where $\|\boldsymbol{x}_0\|_0$ is the number of nonzero components of $\boldsymbol{x}_0$. In the case when $\boldsymbol{x}$ is compressible in $\boldsymbol{\Psi}$, it can be well approximated by the best K-term representation. Consider an $M \times N$ sensing matrix $\boldsymbol{\Phi}$ with $M < N$ and assume that M linear measurements are made such that $\boldsymbol{y} = \boldsymbol{\Phi}\boldsymbol{x} = \boldsymbol{\Phi}\boldsymbol{\Psi}\boldsymbol{x}_0 = \Theta\boldsymbol{x}_0$. Given $\boldsymbol{y}$ and the matrix Θ, the general problem is to recover $\boldsymbol{x}_0$. Since $M < N$, this leads to the problem of solving an underdetermined system of linear equations. A successful way to estimate $\boldsymbol{x}_0$ in this situation is to find the sparsest solution, which can be done by solving the following optimization problem:

$$\min_{\boldsymbol{x}_0} \|\boldsymbol{x}_0\|_0 \quad \text{s.t.} \quad \boldsymbol{y} = \Theta\boldsymbol{x}_0. \tag{9}$$

Unfortunately, the above minimization problem is NP-hard and is computationally difficult to solve. The approach taken in CS theory is to solve a relaxed version of (9)

$$\min_{\boldsymbol{x}_0} \|\boldsymbol{x}_0\|_1 \quad \text{s.t.} \quad \boldsymbol{y} = \Theta\boldsymbol{x}_0 \tag{10}$$

where $\|\cdot\|$ denotes l_1 norm. The optimization problem (10) is often known as basis pursuit (BP) which can be solved by linear programming methods. It has been shown that under certain conditions on Θ and the sparsity of $\boldsymbol{x}_0$, the solutions to both (9) and (10) are the same[6, 7].

In the case of noisy observations of the following form:

$$\boldsymbol{y} = \Theta\boldsymbol{x}_0 + \nu \tag{11}$$

where ν is the noise term, $\|\nu\|_2 \leqslant \varepsilon$, the basis pursuit denoising model can be used to approximate the original signal:

$$\min_{\boldsymbol{x}_0} \|\boldsymbol{x}_0\|_1 \quad \text{s.t.} \quad \|\boldsymbol{y} - \Theta\boldsymbol{x}_0\| \leqslant \varepsilon. \tag{12}$$

Based on CS theory and ISAR signal observation model (8), given compressed echo samples E and sensing matrix $\boldsymbol{\Phi}$, l_1 norm based CS ISAR imaging model can be formulated as

$$\min_{\boldsymbol{a}\in\mathbf{C}^N} \|\boldsymbol{a}\|_1 \quad \text{s.t.} \quad \|E - \boldsymbol{\Phi}\boldsymbol{\Psi}\boldsymbol{a}\|_2 \leqslant \varepsilon \tag{13}$$

where $\boldsymbol{a}$ is the complex-valued amplitude estimator with respect to dictionary $\boldsymbol{\Psi}$ and $\varepsilon = \|\eta\|_2$ is the noise level. The usage of l_1 norm imposes that most elements of $\boldsymbol{a}$ are small with a few large ones, in accordance with the sparsity of the ISAR signal in the RD plane. The l_2 norm inequality constraint preserves the data fidelity of the solution with noise suppression under level ε. This optimization problem can be efficiently solved by YALL1[21], Spgl1[22] and NESTA[23].

3 Gini index based CS ISAR imaging

Different from the common l_1 norm based CS ISAR imaging approaches, we propose an improved CS framework for ISAR imaging using a new sparsity measure named Gini index.

3.1 Gini index

Given a vector $\boldsymbol{a} = [a_1, a_2, \cdots, a_N]$, we order from smallest to largest, $a_{[1]} < a_{[2]} < \cdots < a_{[N]}$, where $[1], [2], \cdots [N]$ are the new indices after the sorting operation. The Gini index of signal $\boldsymbol{a}$ is defined as

$$G(\boldsymbol{a}) = 1 - 2\sum_{i=1}^{N} \frac{|a_{[i]}|}{\|\boldsymbol{a}\|_1}\left(\frac{N - i + 0.5}{N}\right). \tag{14}$$

It is clear that Gini index will increase as the sparsity of the signal increases. Furthermore, there are some important advantages of Gini index over the conventional l_1 norm measures.

1) It is normalized: for any signal $\boldsymbol{a}$, we have $G(\boldsymbol{a}) \in [0, 1]$. We have $G(\boldsymbol{a}) = 0$ for the least sparse signal with all the coefficients having an equal amount of energy; and $G(\boldsymbol{a}) = 1$ for the sparsest one which has all the energy concentrated in just one coefficient.

2) It is independent of the size of the signal, thereby enabling us to compare the sparsity of signals of different sizes.

3) It is scale-invariant and independent of the total energy of the signal: $G(\boldsymbol{a}) = G(c\boldsymbol{a})$, $\forall c \in \mathbf{R}^+$, and thus it is ideally suited for comparing the sparsity of a signal in different transform domains.

4) It depends on the relative distribution of energy among the coefficients, as a fraction of the total energy, and not be calculated based solely on the absolute value of each coefficient.

Here, we reconsider the example given in Section 1 to demonstrate that Gini index is more general and consistent than l_1 norm. The two signals given in Section 1 are $x_1 = (7, 1, 1, 0)$ and $x_2 = (3, 3, 3, 0)$. If we use l_1 norm as the sparsity measure, we find that the sparsity of those two signals is the same ($\|x_1\|_1 = \|x_2\|_1 = 9$). But, if we use the Gini index as the sparsity measure, we have $G(x_1) = 0.4394$, $G(x_2) = 0.25$, and it clearly shows that signal x_1 is sparser than signal x_2. More examples can be found in [15].

The above observations serve as motivations of why we use the Gini index as a sparsity measure in our CS ISAR imaging model. We formulate proposed CS ISAR imaging model as follows.

3.2 Proposed model

Given ISAR signal observation model (8), Gini index based CS ISAR imaging model can be expressed as

$$\max_{\boldsymbol{a}\in\mathbf{C}^N} G(\boldsymbol{a}) \quad \text{s.t.} \quad \|E-\boldsymbol{\Phi}\boldsymbol{\Psi}\boldsymbol{a}\|_2<\varepsilon \tag{15}$$

where $G(\cdot)$ is the Gini index defined in (14), E is the compressed measurements, $\boldsymbol{\Phi}\in\mathbf{C}^{M\times N}$ is the sensing matrix, $\boldsymbol{\Psi}$ is the dictionary defined in (5), $\boldsymbol{a}$ is the scene vector, and ε is dependent on the noise level.

3.3 Iteratively reweighted algorithm

To solve this maximization problem, simultaneous perturbation stochastic approximation (SPSA)[16, 24] was used to seek the solution due to the nonlinearity of Gini index. The essential feature of SPSA, which provides its power and relative ease of use in difficult multivariate optimization problems, is the underlying gradient approximation that requires only two objective function measurements per iteration regardless of the dimension of the optimization problem. However, we find SPSA is usually time-consuming in dealing with the Gini index based ISAR-CS model. To overcome this problem, we find that the Gini index based CS ISAR imaging model can be reformulated into a reweighted l_1 minimizing framework, thus the fast iterative shrinkage thresholding method[25] can be used to seek the optimal solution without stochastic approximation.

Substituting (14) into (15), the problem (15) is equivalent to the following minimization problem:

$$\min_{\boldsymbol{a}\in\mathbf{C}^N}\sum_{i=1}^{N}\left(\frac{N-i+\frac{1}{2}}{N\|\boldsymbol{a}\|_1}\right)|a_{[i]}| \quad \text{s.t.} \quad \|E-\boldsymbol{\Phi}\boldsymbol{\Psi}\boldsymbol{a}\|<\varepsilon. \tag{16}$$

In order to solve the problem efficiently, we rewrite the prior term in (16) in an inner product form:

$$\left[\frac{N-1+\frac{1}{2}}{N\|\boldsymbol{a}\|_1},\frac{N-2+\frac{1}{2}}{N\|\boldsymbol{a}\|_1},\cdots,\frac{N-N+\frac{1}{2}}{N\|\boldsymbol{a}\|_1}\right]\begin{bmatrix}|a_{[1]}|\\|a_{[2]}|\\\vdots\\|a_{[N]}|\end{bmatrix} \tag{17}$$

and it can be viewed as a new weighted l_1-norm which is defined by

$$\left[\frac{N-I_1+\frac{1}{2}}{N\|\boldsymbol{a}\|_1},\frac{N-I_2+\frac{1}{2}}{N\|\boldsymbol{a}\|_1},\cdots,\frac{N-I_N+\frac{1}{2}}{N\|\boldsymbol{a}\|_1}\right]\begin{bmatrix}|a_{[1]}|\\|a_{[2]}|\\\vdots\\|a_{[N]}|\end{bmatrix}\triangleq |W^{\mathrm{T}}(\boldsymbol{a})\boldsymbol{a}|_1 \tag{18}$$

where I_i is the index of element a_i in vector $[a_{[1]},a_{[2]},\cdots,a_{[N]}]$, and the weight vector is defined by

$$W^{\mathrm{T}}(\boldsymbol{a})=\left[\frac{N-I_1+\frac{1}{2}}{N\|\boldsymbol{a}\|_1},\frac{N-I_2+\frac{1}{2}}{N\|\boldsymbol{a}\|_1},\cdots,\frac{N-I_N+\frac{1}{2}}{N\|\boldsymbol{a}\|_1}\right]. \tag{19}$$

Using (16), (17), (18) and (19), the maximization problem (15) can be converted to the following minimization problem:

$$\min_{\boldsymbol{a}\in C^N}|W^{\mathrm{T}}(\boldsymbol{a})\boldsymbol{a}|_1 \quad \text{s.t.} \quad \|E-\boldsymbol{\Phi}\boldsymbol{\Psi}\boldsymbol{a}\|_2\leqslant\varepsilon. \tag{20}$$

Problem (20) is not the same as general weighted l_1-norm minimization problem because the weight $W^{\mathrm{T}}(\boldsymbol{a})$ is related to independent variable $\boldsymbol{a}$ and the objective function $|W^{\mathrm{T}}(\boldsymbol{a})\boldsymbol{a}|_1$ is nonlinear, so we need to design a new algorithm to find the solution.

In this paper, we propose an iteratively reweighted algorithm that alternates between the solution estimation and the weights redefinition. The algorithm is described as follows:

Step 1. Initialize $\tilde{\boldsymbol{a}}=\boldsymbol{a}_0$, ε (which depends on noise level) and $\boldsymbol{W}=W^{\mathrm{T}}(\boldsymbol{a}_0)$.

Step 2. Solve the following minimization problem with the current solution $\tilde{\boldsymbol{a}}$ and the current weight W^{T} using fast iterative shrinkage thresholding method (FIST)[25]:

$$\boldsymbol{a}^*=\arg\min_{\boldsymbol{a}\in\mathbf{C}^N}|\boldsymbol{W}\boldsymbol{a}|_1 \quad \text{s.t.} \quad \|E-\boldsymbol{\Phi}\boldsymbol{\Psi}\boldsymbol{a}\|_2\leqslant\varepsilon.$$

Step 3. Update:

a) Update the weights: $\boldsymbol{W}\leftarrow W^{\mathrm{T}}(\boldsymbol{a}^*)$, where $W^{\mathrm{T}}(\boldsymbol{a}^*)$ is defined by (19);

b) Update the current solution: $\tilde{\boldsymbol{a}}\leftarrow\boldsymbol{a}^*$.

Step 4. Terminate on convergence or the number of iterations attains a given maximum value. Otherwise, go to Step 2.

Here are three comments about the algorithm: 1) It has been shown in [16] that Gini index defined in (14) is quasi-convex in $|\boldsymbol{a}|$. To the best of our knowledge, theoretical analysis of Gini index based reconstruction model is deficient and existence and uniqueness of solution to this model is unknown. We would like to carry out a separate research on this topic in our future work. 2) Because the objective function in (20) is nonlinear and non-convex, it is very hard to give a theoretical guarantee on the convergence of the iterative reweighted algorithm. However, to demonstrate the effectiveness and stability of our iteratively reweighted algorithm, we have tested our algorithm on various data sets, and the results indicated that proposed algorithm is very stable and reliable. 3) In this paper, we terminate our algorithm when relative change of two consecutive iterations becomes small:

$$\frac{\|\tilde{\boldsymbol{a}}-\boldsymbol{a}^*\|_2}{\|\tilde{\boldsymbol{a}}\|_2}<\sigma \tag{21}$$

where $\sigma>0$ is a tolerance. In our experiments we choose $\sigma=10^{-4}$.

4 Experimental results

In order to evaluate the performance of the Gini index based CS ISAR imaging method, several simulated experiments are presented at different SNR level and normalized measurements number $\frac{M}{N}$ in this section. The processing is also implemented for conventional RD algorithm and l_1 norm based CS ISAR imaging method, and the results are compared with those three methods in terms of two indica-

tors: the peak sidelobe ratio (PSLR) and the reconstruction relative error (RE)[26].

PSLR is defined as the ratio of peak intensity of the most prominent sidelobe and the peak intensity of the mainlobe:

$$PSLR = 10\log_{10}\frac{\max\limits_{|x|<\rho_x,|y|<\rho_y}\boldsymbol{a}^2(x,y)}{\max\limits_{\rho_x<|x|<5\rho_x,\rho_y<|y|<5\rho_y}\boldsymbol{a}^2(x,y)} \tag{22}$$

where $\boldsymbol{a}(x,y)$ is the focused image of point-scatter, ρ_x and ρ_y are the half width of mainlobe in range and cross range, respectively.

Relative error of reconstructed image is defined as

$$RE = \left(\frac{\sum\limits_{i=1}^{M}\sum\limits_{j=1}^{N}(\hat{\boldsymbol{a}}(i,j)-\boldsymbol{a}(i,j))^2}{\sum\limits_{i=1}^{M}\sum\limits_{j=1}^{N}(\boldsymbol{a}(i,j))^2}\right)^{\frac{1}{2}} \tag{23}$$

where $\boldsymbol{a}(i,j)$ denotes the ground truth image of scattering coefficients for illuminated scene, and $\hat{\boldsymbol{a}}(i,j)$ is the reconstructed imaging. Obviously, the lower relative error is, the better reconstructed performance will be.

Assume that the target is 4 km away from the radar and rotates with a rotational velocity of 0.0209 rad/s. The starting frequency of transmit signal is $f_0 = 9$ GHz and the bandwidth of transmit signal is $B = 125$ MHz, pulse repetition frequency (PRF) is 35 kHz, the number of pulses and the number of bursts are $m = 128$ and $n = 128$. We list the detailed target and radar parameters in Table 1.

Table 1 Target and radar parameters

Parameter name	Symbol	Value
Target′s initial position in range	R_0	4 km
Target′s rotational velocity	ω	0.0209 rad/s
Starting frequency	f_0	9 GHz
Frequency bandwidth	B	125 MHz
Pulse repetition frequency	F_a	35 kHz
Pulse duration	T_r	1.016 μs
Number of pulses	m	128
Number of bursts	n	128
CPI	T	0.468 s

In our experiments, the simulations of two scenes are tested, one is a very simple scene of some point targets shown in Fig. 2 (a), and another is a complex scene of an airplane shown in Fig. 2 (b). To analyze the influence of noise, in our simulation, the echo signals are added by complex Gaussian white noise with different signal noise ratio (SNR) level.

Fig. 3 shows the imaging results of point targets scene using RD algorithm, l_1 norm based CS ISAR imaging method and Gini index based CS ISAR imaging method with different SNR level (SNR = 10 dB, 20 dB, 30 dB and noise free). Fig. 3 (a) shows the result of RD algorithm, and Fig. 3 (b) and Fig. 3 (c) show the imaging results of l_1 norm based method and the Gini index based method using 10% echo samples, respectively.

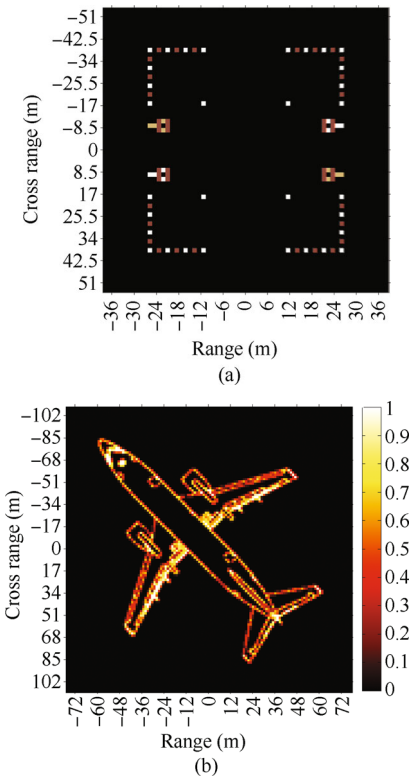

Fig. 2 The original simulated scenes. (a) Point targets; (b) An airplane image

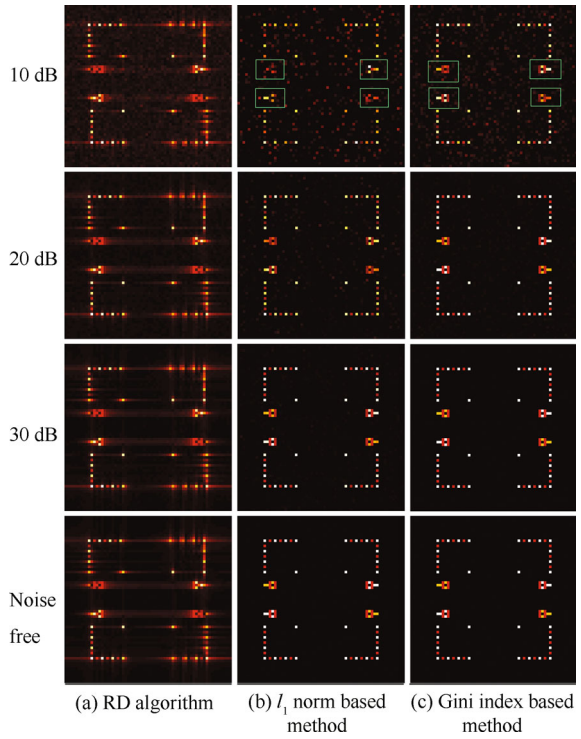

Fig. 3 Images reconstructed by different approaches versus SNR

It can be seen from Fig. 3 (a) that there are serious sidelobes in the results of RD algorithm at all SNR levels. Some details of positions and amplitudes of the targets are missing

or indistinct as the distance between adjacent targets are too close. However, even at very low SNR, RD algorithm obtains almost the same results as at high SNR because match filtering processing can suppress noise effectively.

At high SNR level (SNR > 10 dB), it is observed that the actual target positions and amplitudes are clearly reconstructed by both l_1 norm based method and our method, and the sidelobe in those two methods is far small than that in RD method. Comparing the results in Figs. 3 (b) and (c), we note that the images obtained by our method are cleaner than ones obtained by l_1 norm based method. Even at low SNR level (SNR = 10 dB), our method still offers good performance, while the result of l_1 norm based method are contaminated by noise and false points (highlighted by the white rectangle in first image in Figs. 3 (a) and (b). Those results indicate that our method is more robust to SNR and succeeds in providing image with high quality under low SNR.

To characterize the performance quantitatively, we compute the PSLR value of one point target in Fig. 2 (a) located at range 12 m and cross range −17 m, and show the results in Fig. 4. As shown in Fig. 4, the PSLR value of traditional ISAR images is about 18 dB, while the PSLR value of l_1 norm based method and our method is much larger when SNR > 10. Also, it is clear that our method outperforms l_1 norm based method in terms of PSLR.

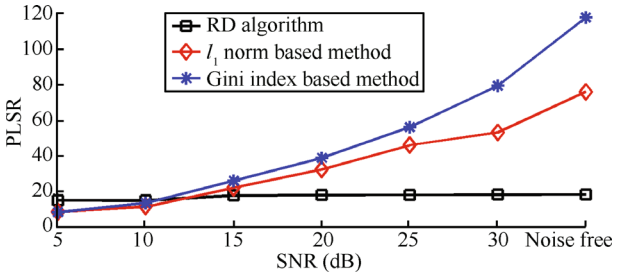

Fig. 4 PLSR values of various methods versus the SNR

Fig. 5 shows the imaging results of the airplane scene by three methods mentioned before with different SNR level (SNR =10 dB, 20 dB, 30 dB and noise free). The original airplane image is shown in Fig. 2 (b). Fig. 5 (a) shows the result of RD algorithm, and Figs. 5 (b) and (c) show the imaging results of l_1 norm based method and the Gini index based method using 25% echo samples, respectively.

As shown in Fig. 5, we can see that: 1) Compared with the traditional ISAR reconstruction results, the proposed method reconstructs higher quality images with reduced sidelobes at much lower sampling rate than Nyquist rate when SNR > 10 dB. 2) The imaging results of two CS methods are contaminated by noise when SNR = 10 dB, and 3) the comparison of the results of l_1 norm based method and our method manifests that our method is more stable and reliable to noise, and more specifically, our method can significantly improve the imaging quality when SNR is above 10 dB.

Furthermore, to analyze the influence of noise quantitatively, imaging results of three methods with different SNR are evaluated in terms of RE value. The detailed results are shown in Fig. 6. It further demonstrates that the presented CS imaging method outperforms RD algorithm and l_1 norm based method when SNR is above 10 dB.

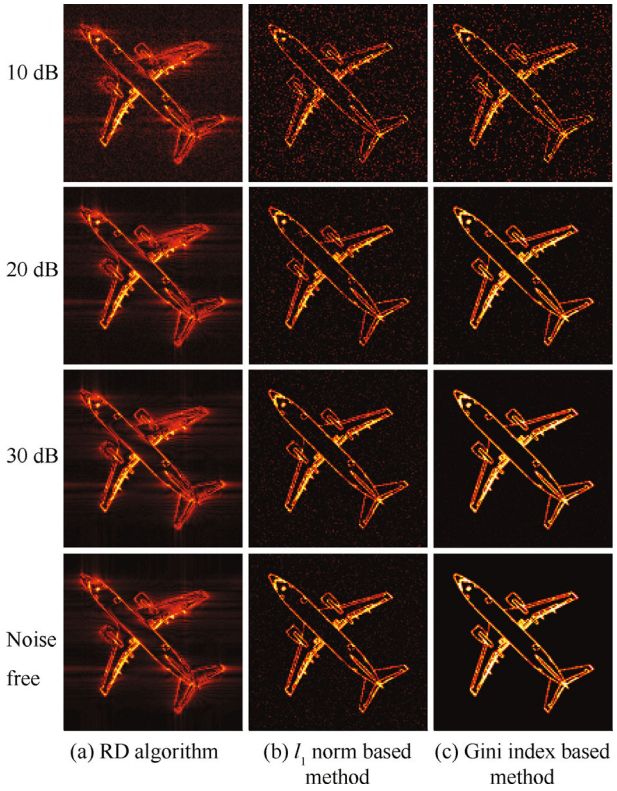

Fig. 5 Images reconstructed by different approaches versus SNR

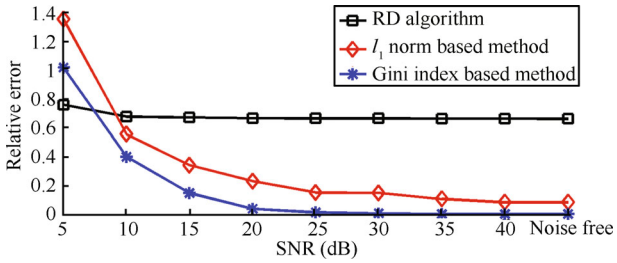

Fig. 6 RE values of various methods versus the SNR

We should point out that the performance of compressive sensing relies on the number of measurements. So in our experiments, we compare the performance of three approaches in the presence of noise versus normalized numbers of measurements $\frac{M}{N}$ (from 10% to 34%). We show the RE value of the imaging results at SNR = 20 dB and 30 dB in Figs. 7 (a) and (b), respectively. Black lines in each figure represent the RE value of the imaging result of RD algorithm with full echo samples.

As demonstrated by Fig. 7, we can see that: 1) The CS method outperforms the RD algorithm when the normalized number of the measurements is more than 0.18, but the performance of our method begins to degrade markedly when the normalized number of the measurements is less than 0.18. 2) Gini index based method produces high-quality images with lower RE values than l_1 norm based method. 3) The proposed method needs fewer measurements to implement ISAR imaging effectively, and the req-

uisite number of measurements for exact reconstruction is dropped from about 30% to about 22%.

The experimental results tell that Gini index based CS ISAR imaging formations are suitable for the construction of ISAR images with very limited number of pulses.

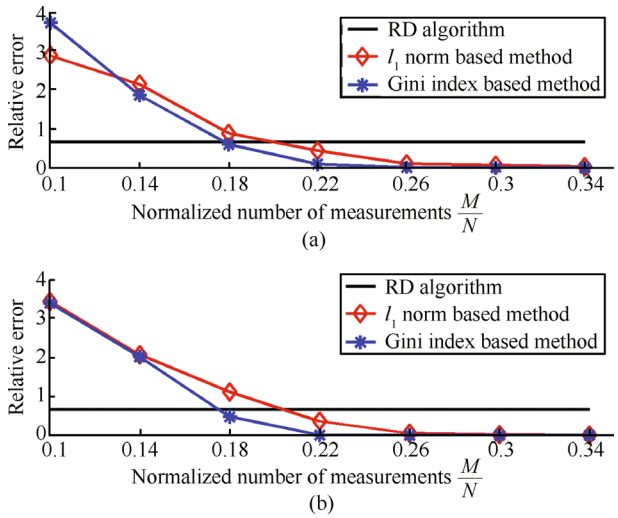

Fig. 7 RE values of various methods versus the number of measurements at different SNR level. (a) SNR = 20 dB; (b) SNR = 30 dB

5 Conclusions

The performance of CS ISAR imaging is significantly dependent on the number of measurements and the noise level. This paper presents an enhanced sparse reconstruction method for CS ISAR imaging based on Gini index, which can sustain strong clutter noise and provide high quality images with extremely limited measurements. The essence of our method is the utilization of Gini index as the sparsity measure in CS imaging. An iteratively reweighted algorithm is applied to solve the proposed model suppressing noise. Our experiments show that the Gini index based CS ISAR imaging approach achieves better performance than other formulations, and it is very robust in the presence of noise. It is believed that its robustness to suppress noise and light requirement of measurements make it useful in real applications of ISAR imaging.

References

[1] C. Özdemir. *Inverse Synthetic Aperture Radar Imaging with MATLAB Algorithms*, Hoboken, NJ: John Wiley & Sons, 2012.

[2] M. Cheney, B. Borden. *Fundamentals of Radar Imaging*, Philadelphia, USA: SIAM, 2009.

[3] X. H. Yang, L. C. Jiao, D. F. Li. Directional filter for SAR images based on nonsubsampled contourlet transform and immune clonal selection. *International Journal of Automation and Computing*, vol. 6, no. 3, pp. 245–253, 2009.

[4] V. C. Chen, S. Qian. Joint time-frequency transform for radar range-Doppler imaging. *IEEE Transactions on Aerospace and Electronic Systems*, vol. 34, no. 2, pp. 486–499, 1998.

[5] J. S. Son, G. Thomas, B. C. Flores. *Range-Doppler Radar Imaging and Motion Compensation*, Boston, MA: Artech House, 2001.

[6] E. J. Candés, J. K. Romberg, T. Tao. Robust uncertainty principles: Exact signal reconstruction from highly incomplete frequency information. *IEEE Transactions on Information Theory*, vol. 52, no. 2, pp. 489–509, 2006.

[7] D. L. Donoho. Compressed sensing. *IEEE Transactions on Information Theory*, vol. 52, no. 4, pp. 1289–2306, 2006.

[8] E. J. Candes, M. B. Wakin. An introduction to compressive sampling. *IEEE Signal Processing Magazine*, vol. 25, no. 2, pp. 21–30, 2008.

[9] M. A. Herman, T. Strohmer. High-resolution radar via compressed sensing. *IEEE Transactions on Signal Processing*, vol. 57, no. 6, pp. 2275–2284, 2009.

[10] J. H. G. Ender. On compressive sensing applied to radar. *Signal Processing*, vol. 90, no. 5, pp. 1402–1414, 2010.

[11] L. Zhang, M. D. Xing, C. W. Qiu, J. Li, Z. Bao. Achieving higher resolution ISAR imaging with limited pulses via compressed sampling. *IEEE Geoscience and Remote Sensing Letters*, vol. 6, no. 3, pp. 567–571, 2009.

[12] L. Zhang, M. D. Xing, C. W. Qui, J. Li, J. L. Sheng, Y. C. Li, Z. Bao. Resolution enhancement for inversed aperture radar imaging under low SNR via improved compressive sensing. *IEEE Transactions on Geoscience and Remote Sensing*, vol. 48, no. 10, pp. 3824–3838, 2010.

[13] H. X. Wang, Y. H. Quan, M. D. Xing, S. H. Zhang. ISAR imaging via sparse probing frequencies. *IEEE Geoscience and Remote Sensing Letters*, vol. 8, no. 3, pp. 451–455, 2011.

[14] G. H. Zhao, Z. Y. Wang, Q. Wang, G. M. Shi, F. F. Shen. Robust ISAR imaging based on compressive sensing from noisy measurements. *Signal Processing*, vol. 92, no. 1, pp. 120–129, 2012.

[15] N. Hurley, S. Rickard. Comparing measures of sparsity. *IEEE Transactions on Information Theory*, vol. 55, no. 10, pp. 4723–4741, 2009.

[16] D. Zonoobi, A. A. Kassim, Y. V. Venkatesh. Gini index as sparsity measure for signal reconstruction from compressive samples. *IEEE Journal of Selected Topics in Signal Processing*, vol. 5, no. 5, pp. 927–932, 2011.

[17] C. Feng, L. Xiao, Z. H. Wei. Compressive sensing ISAR imaging with stepped frequency continuous wave via Gini sparsity. In *Proceedings of IEEE International Geoscience and Remote Sensing Symposium*, IEEE, Melbourne, Australia, pp. 2063–2066, 2013.

[18] Y. X. Wang, H. Ling, V. C. Chen. ISAR motion compensation via adaptive joint time-frequency technique. *IEEE Transactions on Aerospace and Electronic Systems*, vol. 34, no. 2, pp. 670–677, 1998.

[19] J. F. Wang, D. Kasilingam. Global range alignment for ISAR. *IEEE Transactions on Aerospace and Electronic Systems*, vol. 39, no. 1, pp. 351–357, 2003.

[20] T. Thayaparan, L. Stankovic, C. Wernik, M. Dakovic. Real-time motion compensation, image formation and image enhancement of moving targets in ISAR and SAR using S-method based approach. *IET Signal Processing*, vol. 2, no. 3, pp. 247–264, 2008.

[21] J. F. Yang, Y. Zhang. Alternating direction algorithms for L_1-problems in compressive sensing. *SIAM Journal on Scientific Computing*, vol. 33, no. 1, pp. 250–278, 2011.

[22] E. Van Der Berg, M. P. Friedlander. Probing the Pareto frontier for basis pursuit solutions. *SIAM Journal on Scientific Computing*, vol. 31, no. 2, pp. 890–912, 2008.

[23] S. Becker, J. Bobin, E. J. Candés. NESTA: A fast and accurate first-order method for sparse recovery. *SIAM Journal on Imaging Sciences*, vol. 4, no. 1, pp. 1–39, 2011.

[24] A. T. Abdulsadda, K. Iqbal. An improved SPSA algorithm for system identification using fuzzy rules for training neural networks. *International Journal of Automation and Computing*, vol. 8, no. 3, pp. 333–339, 2011.

[25] A. Beck, M. Teboulle. A fast iterative shrinkage-thresholding algorithm for linear inverse problems. *SIAM Journal on Imaging Sciences*, vol. 2, no. 1, pp. 183–202, 2009.

[26] S. J. Wei, X. L. Zhang, J. Shi, G. Xiang. Sparse reconstruction for SAR imaging based on compressed sensing. *Progress in Electromagnetics Research*, vol. 109, no. 1, pp. 63–81, 2010.

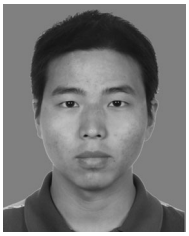

Can Feng received his B. Sc. degree in applied mathematics from Nanjing University of Science & Technology, China in 2007. He is currently a Ph. D. candidate in the School of Computer Science and Engineering of Nanjing University of Science & Technology, China.

His research interests include image processing, radar signal processing, compressive sensing and its application in image processing.

E-mail: fengcan2004@126.com (Corresponding author)

Liang Xiao received his B. Sc. and M. Sc. degrees in applied mathematics, and his Ph. D. degree from Nanjing University of Science and Technology, China. He is currently a professor and doctoral supervisor of Nanjing University of Science and Technology, China.

His research interests include variational partial differential equation (PDE) application in image processing, image modeling, pattern recognition, motion estimation and tracking, virtual reality, and system simulation.

E-mail: xtxiaoliang@163.com

Zhi-Hui Wei received his B. Sc. and M. Sc. degrees in mathematics from Southeast University, China in 1983 and 1986, respectively. He received his Ph. D. degree in communication and information system from Southeast University, China in 2003. He is currently a professor and doctoral supervisor of Nanjing University of Science and Technology, China.

His research interests include mathematical image processing/signal processing, image modeling, multi-scale analysis, video and image coding and compressing, watermarking and steganography, and speech and audio processing.

E-mail: gswei@mail.njust.edu.cn